

Thermodynamics and Synthesis of AlN-Reinforced Mg Alloy Composites



RAMANA G. REDDY

In situ synthesis of aluminum nitride (AlN)-reinforced magnesium alloy composites using ammonia (NH₃) gas was investigated. Feasibility of *in situ* formation of AlN reinforcement was analyzed based on Gibbs energy minimization method. Thermodynamic analysis showed that AlN forms in Mg–Al alloy in the temperature range from 923 K to 1223 K and the oxygen that may be present in the system was detrimental for the formation of nitrides. The thermodynamic analysis also shows that Mg aids in decreasing the oxygen content from the system. Injecting ammonia gas through Mg alloy caused bulk nitridation of the alloy, which led to the formation of AlN-reinforced Mg alloy composites. Presence of hydrogen, which was generated by the dissociation of ammonia, in the alloy getters the trace oxygen in the gaseous precursor, enabling the formation of AlN. For the ammonia injection through the Mg–Al alloy containing 30 wt pct Al at 1173 K and injection time of 70 minutes, the yield of AlN was found to increase with an increase in the flow rate of ammonia. The AlN formed in the melt was 15.42 wt pct AlN for a gas flow rate of 0.04 LPM (liters per minute), and 27.43 wt pct AlN at a flow rate of 0.1 LPM. AlN particles formed *in situ* are surrounded by the γ -(Mg, Al) phase. X-ray diffraction characterization showed that the composites formed *in situ* were composed of (Mg), intermetallic γ -(Mg, Al), and AlN phases. Scanning electron microscopy and optical microscopy analyses revealed that the AlN particles formed *in situ*, dispersed uniformly, and the increase in flow rate increases the dispersion density of AlN particles in the composites. The experimental compositions and phases obtained are included in the constructed Mg–Al–N ternary phase diagram at 1173 K. All experimental data fall in the region of AlN and Mg–Al alloy, which is in validation with the thermodynamic prediction. The experimental obtained amount of AlN in composites as a function of Al content in alloy are in good agreement with the thermodynamic modeled results, which indicates that the formation of AlN in Mg–Al alloy is close to an equilibrium process.

<https://doi.org/10.1007/s11663-024-03100-7>

© The Minerals, Metals & Materials Society and ASM International 2024

I. INTRODUCTION

METAL matrix composites (MMCs) have immense potential for automotive and aerospace applications. Currently, they are in use for the space shuttles, electronic substances, bicycles, commercial airlines, automobiles, golf clubs, and a variety of applications. This is because reinforcing the matrix with the hard ceramic phases improves the wear resistance, tensile strength, and elastic modulus of the metallic materials. Discontinuously reinforced metal/alloy composites (DRACs) have been the most promising manufacturing

technology for the MMCs. While majority are aluminum matrix composites, growing number of applications require the matrix properties of lightweight alloys, such as magnesium and titanium. Magnesium composites and their applications have been reviewed.^[1–7] The mechanical properties, grain refinement by ceramic particles additives, and corrosion of magnesium alloys were reported.^[8–17] There have been very few efforts which concentrated on the processing and properties of MMCs using magnesium and its alloys as the matrices.^[18–25] Magnesium has lower density (about 1.74 g/cm³) and comparable stiffness-to-weight ratio, in comparison to aluminum which makes magnesium and its alloys as excellent candidates for matrix materials for MMCs. The global use of magnesium in automobile parts is estimated to increase about 15 pct annually.

MMCs are primarily produced using solidification and powder metallurgy methods. In solidification method, the reinforcements are introduced into the molten metals using conventional foundry processes. In

RAMANA G. REDDY is with the Department of Metallurgical and Materials Engineering, The University of Alabama, Tuscaloosa, AL 35487. Contact e-mail: rreddy@eng.ua.edu

Manuscript submitted June 1, 2023; accepted April 6, 2024.

powder metallurgy method, the matrix metal and reinforcement powders are mixed, consolidated, and sintered to form the composites. Squeeze casting,^[18] stir casting,^[19–22] powder metallurgy,^[23] and spray forming^[24] have been studied to produce magnesium MMCs reinforced with SiC. Magnesium MMCs obtained from these conventional techniques have demonstrated the strong potential for weight-critical applications. However, they are still expensive and not profitable for large-scale engineering applications. Prohibitive cost of these composites is associated with synthesizing small size reinforcing particles for the superior mechanical properties of MMCs. In the conventional techniques, the surface of reinforcing particles prepared separately is often contaminated. Hence contamination may lower the thermal and chemical stability of the interfaces within the composites. During the service and secondary processing, MMCs may experience elevated temperature, resulting in phase transformation and interfacial chemical interaction, which might cause thermodynamic instability at the interfaces.

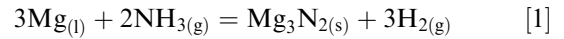
In situ processing, where the reinforcing particles are directly formed from *in situ* chemical reactions, is a promising technology for MMCs manufacturing.^[26] Since the reinforcing particles are formed *in situ*, the production cost of MMCs could be significantly lowered. Since the *in situ* formed reinforcement is thermodynamically stable and free of surface contamination, the stability of the interface can also be notably improved. *In situ* processing of MMCs can be realized by approaches such as solid–solid reaction process, solid-liquid reaction process, direct metal oxidization process, and gas-injection method. *In situ* gas-injection method, in which the reinforcing particles are formed by the reaction between the injected gas and matrix melt, is a potential MMC manufacturing technology. Using this technique, aluminum alloy composites reinforced with TiC,^[27] SiC,^[28,29] and AlN^[30–34] have been successfully produced. Synthesis of magnesium alloy composites reinforced with AlN by gas-injecting method has been presented in our paper.^[35] The additional advantage of this method is that the forced agitation due to the injecting of gas improves the uniformity of dispersion of reinforcement and availability of large gas–liquid contact area which provides fast reaction kinetics.

This paper presents thermodynamic analysis and experimental results on the use of this *in situ* gas-injecting method for producing AlN-reinforced Mg alloy composites using ammonia as the gaseous precursor.

II. THERMODYNAMIC ANALYSIS

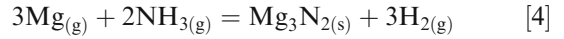
A. Gibbs Energy Minimization Method

Thermodynamic analysis was performed to predict the feasibility and optimum conditions for the formation of AlN in the proposed Mg–Al–NH₃ system.^[36,37] In the Mg–Al–NH₃ system, at temperatures above the liquidus range of Mg–Al alloy, the nitridation reactions and their Gibbs energy changes are given as follows:



$$\Delta G_{(1)} = \Delta G_{(1)}^\circ + RT \ln \left(\frac{P_{\text{H}_2}^3}{a_{\text{Mg}}^3 P_{\text{NH}_3}^2} \right) \quad [2]$$

$$\Delta G_{(1)}^\circ = -377750 - 0.3T \quad \text{J} \quad (923 < T < 1223 \text{ K}) \quad [3]$$



$$\Delta G_{(4)} = \Delta G_{(4)}^\circ + RT \ln \left(\frac{P_{\text{H}_2}^3}{P_{\text{Mg}}^3 P_{\text{NH}_3}^2} \right) \quad [5]$$

$$\Delta G_{(4)}^\circ = -771021 + 290.15T \quad \text{J} \quad (923 < T < 1223 \text{ K}) \quad [6]$$



$$\Delta G_{(7)} = \Delta G_{(7)}^\circ + RT \ln \left(\frac{P_{\text{H}_2}^3}{a_{\text{Al}}^2 P_{\text{NH}_3}^2} \right) \quad [8]$$

$$\Delta G_{(7)}^\circ = -548116 + 1.0593T \quad \text{J} \quad (923 < T < 1223 \text{ K}) \quad [9]$$



$$\Delta G_{(10)} = \Delta G_{(10)}^\circ + RT \ln \left(\frac{a_{\text{Mg}}^3}{a_{\text{Al}}^2} \right) \quad [11]$$

$$\Delta G_{(10)}^\circ = -169123 - 0.41T \quad \text{J} \quad (923 < T < 1223 \text{ K}) \quad [12]$$

where $\Delta G_{(1)}^\circ, \Delta G_{(4)}^\circ, \Delta G_{(7)}^\circ$, and $\Delta G_{(10)}^\circ$ are the standard Gibbs energy change for the reactions shown in Eqs. [1], [4], [7] and [10], respectively. These are calculated using thermodynamic database.^[36,37] P_{NH_3} is the partial pressure of ammonia in the system, approximately equal to 1 atm for an open system; P_{H_2} is the partial pressure of hydrogen gas which comes from the dissociation of ammonia, approximately equal to 1.5 atm based on the molar balance; and a_{Mg} and a_{Al} are the activities of magnesium and aluminum, respec-

tively. P_{Mg} is the partial pressure of magnesium. The relationship between vapor pressure of Mg against temperature is given as follows:^[38]

$$\log(P_{\text{Mg}}) = \frac{-6.181 \times 10^3}{T} + 6.99 \quad [13]$$

In Eq. [13], P_{Mg} is vapor pressure of magnesium in kPa, and T is temperature in Kelvin. For calculating the Gibbs energy changes of reactions as shown in Eqs. [2], [5], [8] and [11], the activities of Mg and Al are needed. The activities of Mg and Al were calculated using FactSage.^[39] The activity coefficients of Al and Mg were modeled as a function of temperature and composition and are shown as follows:

$$\ln(\gamma_{\text{Al}}) = (0.05159 - 561.27/T) (1 - x_{\text{Al}})^2 \quad [14]$$

$$\ln(\gamma_{\text{Mg}}) = (0.05159 - 561.27/T) (x_{\text{Al}})^2, \quad [15]$$

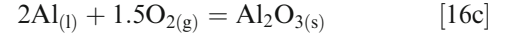
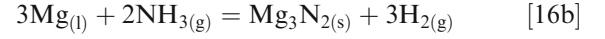
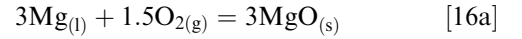
where γ_{Al} is activity coefficient of Al, γ_{Mg} is activity coefficient of Mg, x_{Al} is molar concentration of Al in the melt, and T is temperature in Celsius. The results from FactSage at 1173 K were compared with those fitted using Eqs. [14] and [15] and are shown in Figure 1. A good agreement between the two curves indicates that Eqs. [14] and [15] can be used for determining activity coefficient of Al and Mg at other temperatures and mole fractions.

Based on Eqs. [1] through [15], Gibbs energy change for nitridation of Mg-30 wt pct Al alloy with ammonia as the gaseous precursor was calculated. The calculated results are shown in Figure 2. The Gibbs energy change of the reactions given by Eq. [7] is more negative than those given by Eqs. [1] and [4], implying that nitridation of Al has the preference over nitridation of Mg when using NH_3 as the gas. Nitridation of Mg can take place in both liquid and gaseous state; however, nitridation in gaseous state has higher negative Gibbs energy change than that in liquid state. The above thermodynamic analysis shows that Mg_3N_2 formed in the Mg-Al melt as an intermediate product that could be reduced by Al *via* the reaction given by Eq. [10]. Although nitridation of both magnesium and aluminum is possible, AlN is the only equilibrium product in the melt.

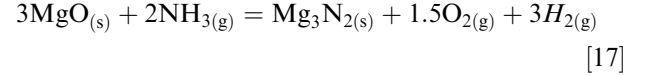
B. Critical Oxygen Content for Nitridation

The chemical affinity between oxygen and Mg or Al is larger than that between nitrogen and Mg or Al. Oxides are the undesirable species in the product phase, as they will change its composition and will degrade the composite. Minimum oxygen content or the critical oxygen partial pressure in the system must be considered and should be controlled for the successful completion of nitridation reactions. This can be obtained by considering the various reactions occurring in the system.

In the temperature range from 923 K to 1223 K, the following reactions are thermodynamically feasible:

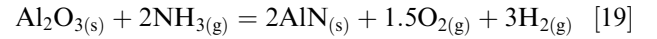


Simplifying Eqs. [16a] and [16b] yields the following reaction:



$$\Delta G_{(17)}^\circ = -347.03T + 1448035 \text{ J} \quad [18]$$

Similarly, simplifying Eqs. [16c] and [16d] yields the following reaction:



$$\Delta G_{(19)}^\circ = -331.003T + 1144394 \text{ J} \quad [20]$$

where ΔG° is the standard Gibbs energy change of the reactions. ΔG° of these reactions can also be expressed from basic principles as follows:

$$\Delta G_{(17)}^\circ = -RT \ln K_{P_{(17)}}^\circ = -RT \ln \left[\frac{\left(\frac{P_{\text{H}_2}}{P^\circ}\right)^3 \times \left(\frac{P_{\text{O}_2}}{P^\circ}\right)^{1.5}}{\left(\frac{P_{\text{NH}_3}}{P^\circ}\right)^2} \right] \quad [21]$$

$$\Delta G_{(19)}^\circ = -RT \ln K_{P_{(19)}}^\circ = -RT \ln \left[\frac{\left(\frac{P_{\text{H}_2}}{P^\circ}\right)^3 \times \left(\frac{P_{\text{O}_2}}{P^\circ}\right)^{1.5}}{\left(\frac{P_{\text{NH}_3}}{P^\circ}\right)^2} \right], \quad [22]$$

where R is $8.314 \text{ JK}^{-1}\text{mol}^{-1}$, P° is 101.325 kPa (1 atm), and P_{H_2} , P_{O_2} , and P_{NH_3} are the gas pressures of hydrogen, oxygen, and ammonia, respectively. The partial pressures of nitrogen and hydrogen are 0.5 and 1.5 times the pressure of ammonia gas, respectively, since they are generated from the dissociation of ammonia. The ammonia dissociates completely into hydrogen and nitrogen at a temperature of 673 K. In the experiment, we have used a pressure of 110.343 kPa (1.089 atm) of ammonia. For ammonia with a pressure of 110.343 kPa, the partial pressure of nitrogen is 55.172 kPa and of hydrogen is 165.515 kPa, respectively, after dissociation.

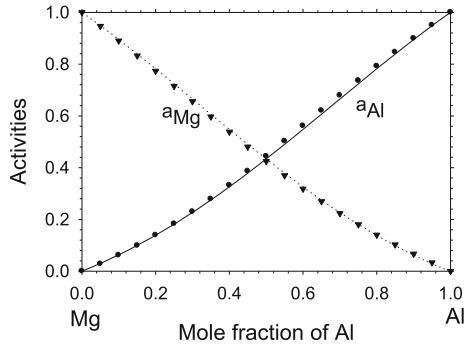


Fig. 1—Comparison of activities of Mg and Al at 1173 K; (black circle) a_{Al} from available data in FactSage, (solid line) a_{Al} from modeled equation,^[14] (black down point triangle) a_{Mg} from available data in FactSage and (dotted line) a_{Mg} from modeled equation.^[15]

Using Eqs. [18], [20], [21] and [22], the critical oxygen partial pressure for the formation of Mg_3N_2 and AlN can be calculated. At 1173 K, the critical oxygen partial pressures for the formation of Mg_3N_2 and AlN are 5.23×10^{-27} and 1.52×10^{-18} Pa, respectively. Figure 3 shows the plot of $\ln P_{\text{O}_2}$ vs $10000/T$. The following observations can be deduced from Figure 3:

- The critical oxygen partial pressure to form AlN is higher than that to form Mg_3N_2 .
- The critical oxygen partial pressures increase with an increase in temperature, which helps to realize the nitridation reaction.

In the region below line A in Figure 3, AlN can form readily. The region below line B is the favorable region for both AlN and Mg_3N_2 formation. The region between line A and B denotes the P_{O_2} and temperature at which AlN will form but not Mg_3N_2 . At a P_{O_2} and temperature in the above region that if Mg_3N_2 can be obtained, then, AlN must be formed.

C. Decrease of Oxygen Content by Magnesium

Magnesium and magnesium vapor may react with oxygen so as to decrease the oxygen content in the system. Before molten Mg–Al alloys reacted with NH_3 , vaporized Mg can react with oxygen to form MgO as shown by the following reaction:



$$\Delta G_{(23)}^\circ = 115.8T - 608683 \text{ J} \quad [24]$$

Magnesium in liquid form can also react with oxygen as shown by the reaction:



$$\Delta G_{(25)}^\circ = 212.52T - 739853 \text{ J} \quad [26]$$

ΔG° of these reactions can be expressed from basic principles as follows:

$$\Delta G_{(23)}^\circ = -RT \ln K_{P_{(23)}}^\circ = -RT \ln \left[\frac{1}{(P_{\text{O}_2})^{0.5} \times (P_{\text{Mg}})^1} \right] \quad [27]$$

$$\Delta G_{(25)}^\circ = -RT \ln K_{P_{(25)}}^\circ = -RT \ln \left[\frac{1}{(P_{\text{O}_2})^{0.5} \times (a_{\text{Mg}})^1} \right] \quad [28]$$

Equations [13], [15], [24], [26], [27] and [28] can be solved to calculate the P_{O_2} . The curve of $\ln P_{\text{O}_2}$ vs $10000/T$ is shown in Figure 4. At 1173 K and for an alloy composition of Mg-30 wt pct Al, P_{O_2} is calculated to be 1.74×10^{-42} Pa for $\text{Mg}_{(\text{l})}$ and 7.35×10^{-54} Pa for $\text{Mg}_{(\text{g})}$. The following observations can be deduced from Figure 4:

- Magnesium significantly decreases the oxygen content in the reaction system.
- Comparing P_{O_2} with the minimum oxygen content for the nitridation reaction of Mg and Al shown in Figure 3, it can be found that the P_{O_2} in the reaction system is lower than the minimum oxygen content required by the nitridation reaction at the same temperature.

III. EXPERIMENTAL

A. Experimental Set-up and Procedure

The experiments were conducted in the vertical tube resistance furnace with a temperature range from 773 K to 1773 K, as shown in Figure 5. The furnace consists of a working chamber, heating elements, insulation, a standard type-S (Pt-10 pct Ru /Pt) thermocouple, and a control console. In the furnace, an overall 14 cm constant temperature zone with a variation of ± 5 K can be obtained.

The alloy composition chosen was 30 wt pct Al and balance Mg. Pure Mg rods (99.9 pct purity, purchased from Good Fellow Corp.[®]) and Al granules (99.99 pct purity, purchased from Alfa Aesar[®]) were used to make the desired alloy composition. Mg and Al were mixed in the alumina crucible with a capacity of 100 ml to obtain the required composition of alloy and the crucible was then placed in the furnace tube in constant temperature zone. Inert atmosphere was created in the reaction chamber by purging it with ultrapure argon of 99.999 pct purity. On reaching the predetermined temperature, the alloy was maintained at constant temperature for about 15 minutes for homogenization. Then the injecting tube was submerged into the melt up to the bottom of the crucible and the injecting gas was introduced into the melt. After injecting gas for a predetermined time, the furnace was turned off, and the products were allowed to cool in the furnace under inert argon atmosphere.

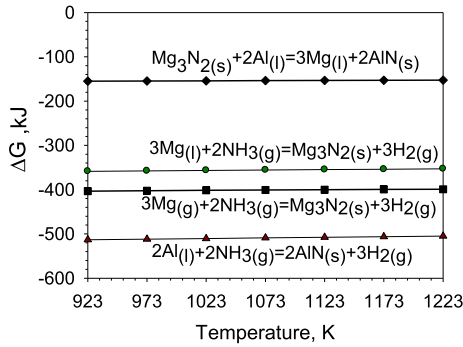


Fig. 2—Gibbs energy change for nitridation reactions of Mg-30 wt pct Al alloy in the temperature range from 923 K to 1223 K using ammonia gas.

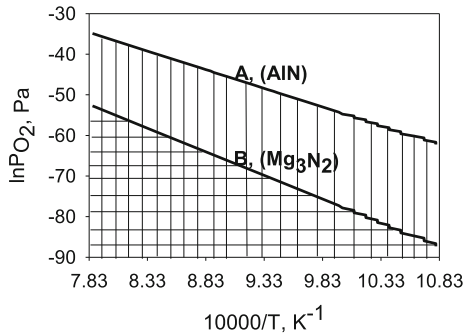


Fig. 3— $\ln P_{O_2}$ vs $10000/T$ for AlN denoted by line A and for Mg_3N_2 denoted by line B.

The reaction crucible was taken out of the furnace for characterizing the products after it was cooled to room temperature in the furnace. The microstructures of the composite were characterized using Scanning Electron Microscopy (SEM-EDS) and Optical Microscopy (OM), and X-Ray Diffraction (XRD) techniques.

IV. RESULTS AND DISCUSSION

Ammonia was bubbled through Mg-30 wt pct Al alloy at 1173 K for 70 minutes at a flow rate of 0.04 LPM (liters per minute). The oxygen content in the injecting gas was 10^{-4} Pa, which is above the minimum oxygen content required for the nitridation reaction as can be seen from Figure 3. At this high content of oxygen, Figure 3 shows that AlN cannot be prepared. Also, Mg_3N_2 cannot be prepared because its critical oxygen partial pressure of formation is lower than that for the formation of AlN.

However, XRD analysis shown in Figure 6 gives convincing evidence that yellow green Mg_3N_2 powder was observed during experiment. Mg_3N_2 powder was found on the reaction products after cooling. It was also collected from the exit gas tube in powder form of greenish-yellow color. The Mg_3N_2 formed in the Mg–Al

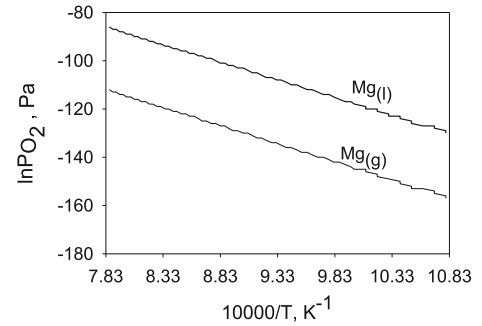


Fig. 4— $\ln P_{O_2}$ vs $10000/T$ for Mg reactions in liquid and gaseous states.

melt that could be reduced by Al *via* the reaction given by Eq. [10]. Thus, it is not retained in the resulting product, *i.e.*, AlN-Mg alloy composite.

The XRD spectrum of reaction product of the (Mg–Al)–AlN composite is shown in Figure 7. The composite was formed *in situ* by injecting NH_3 for 70 minutes through the Mg-30 wt pct Al melt at 1173 K at a flow rate of 0.04 LPM. Similar XRD patterns were obtained for the samples taken from the other parts of the crucible. The phases were identified to be Mg solid solution (aluminum dissolved in it), γ -(Mg, Al) or $Mg_{17}Al_{12}$ and AlN. The composite product weight was found less than the initial weight of raw materials taken which is because of the weight loss of Mg due to vaporization. EDS and XRD analyses show that the average percentage of AlN is about 15.42 wt pct in the product. The percentage of AlN was calculated from XRD data^[40] and EDS data. The results are showed in Figure 10. This AlN percentage is equal to an average weight of 11.19 g of AlN formed in the starting alloy weight of 70 g. About 5.22 g of Mg is lost from the alloy in the form of $Mg_{(g)}$ and in the formation of Mg_3N_2 which is collected from the outlet gas tube in the form of greenish-yellow powder. The XRD of Mg_3N_2 is shown in Figure 6. This Mg_3N_2 was not found as a phase in the bulk product as discussed in the thermodynamics section above, confirming that it is not stable in the alloy.

The presence of Mg_3N_2 from Figure 6 and AlN from Figure 7 shows that the expected oxygen content for nitridation reactions was achieved. As discussed in the thermodynamic section, if Mg_3N_2 can be obtained, then, AlN must be formed, which agrees with the experimental results. Therefore, the key role of magnesium in the formation of AlN can be realized. In the reaction system Mg–Al– NH_3 , other than magnesium, the liberated hydrogen from ammonia also acts as an oxygen getter, so reducing the oxygen content of the melt.

Figure 8 shows the SEM images of the (Mg–Al)–AlN composite formed *in situ*. The EDS analysis of the corresponding to the regions labeled in Figure 8 reveals that the bright particles are AlN, the dark color region is Mg-rich α -phase, and the massive gray domain surrounding the AlN particles is the γ -(Mg, Al). From SEM

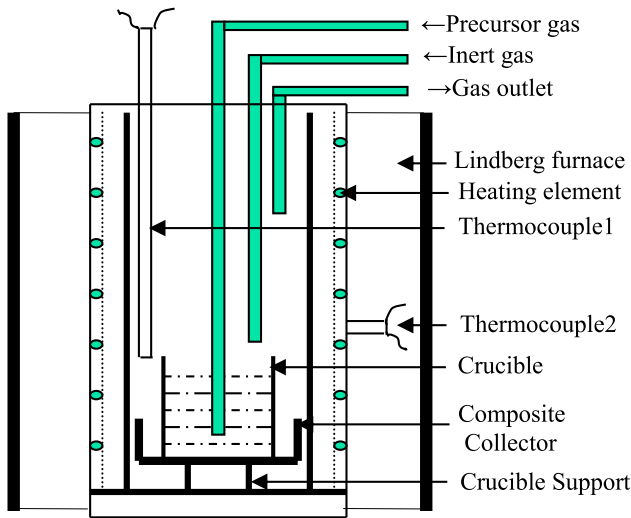


Fig. 5—Schematic diagram of experimental setup.

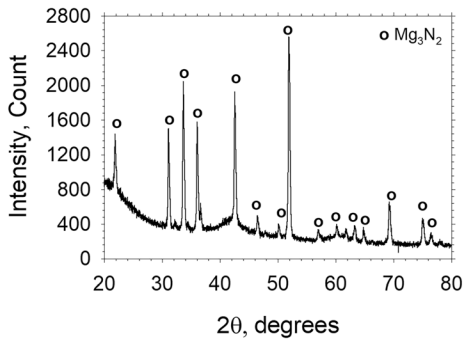


Fig. 6—XRD pattern of Mg_3N_2 .

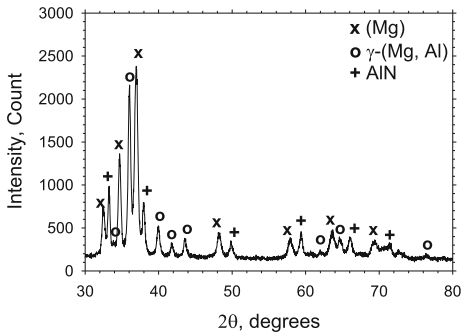


Fig. 7—XRD pattern of product formed after injecting Mg–Al alloy with NH_3 .

micrographs it can be seen that AlN particles are dispersed uniformly throughout the product and are surrounded by the gamma phase.

Figure 9 shows the optical micrographs of the products formed. The composite was formed *in situ* by injecting NH_3 for 70 minutes through the Mg-30 wt pct Al melt at 1173 K at a flow rate of 0.04 LPM. The gray matrix is (Mg) phase, white is γ -(Mg, Al) and the black particles are the AlN particles, which are uniformly

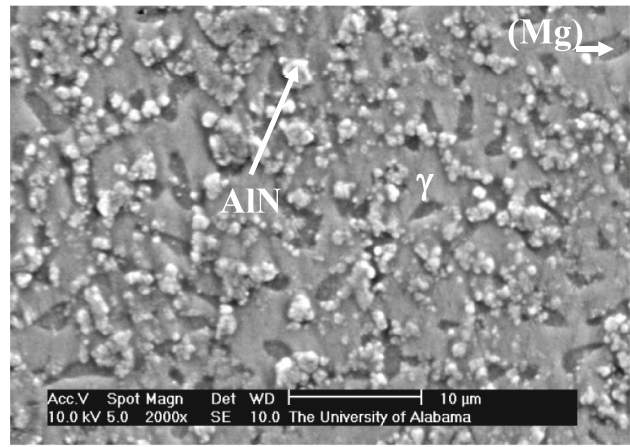


Fig. 8—SEM images of Mg-30 wt pct Al/AlN product.

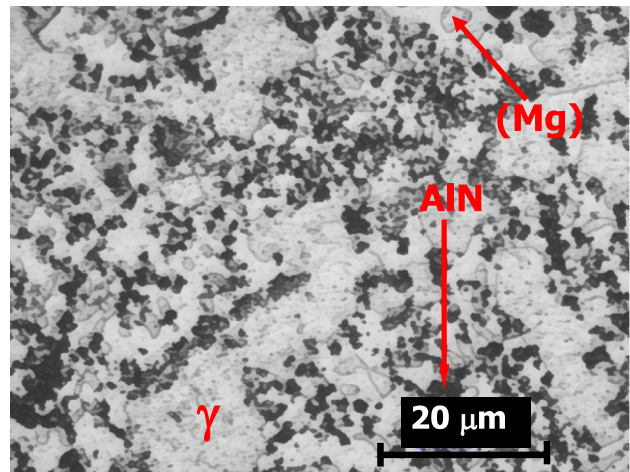


Fig. 9—Optical micrograph of product after injecting with ammonia.

distributed throughout the composite. These optical micrographs also confirm that AlN particles formed *in situ* are small in size.

Zheng and Reddy discussed the case for formation of AlN in aluminum alloys in the gas-injection system with ammonia as the injecting gas.^[32] Their studies indicate that ammonia is not stable and dissociates into nitrogen and hydrogen gases. The nitrogen gas from dissociation is the nitrogen precursor. Therefore, the mechanism of AlN formation is the same as the case using nitrogen gas. Similarly, the mechanism of AlN formation in the Mg–Al alloys using ammonia gas may be the same as the case using nitrogen gas in the present work. AlN may be formed by first nitridation of magnesium and then the reduction of Mg_3N_2 by aluminum. Nitridation reactions may also benefit from the presence of hydrogen similar to nitridation of aluminum in Al– NH_3 system.^[32] Using ammonia accelerates the nitridation of aluminum and therefore the formation of AlN in the Mg–Al– NH_3 system. The above results were obtained for the ammonia gas flow rate of 0.04 LPM. Effect of

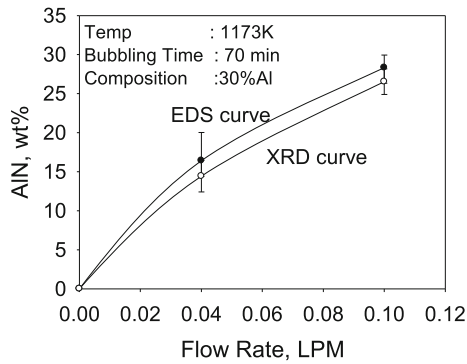


Fig. 10—Effect of flow rate on percentage of AlN yield.

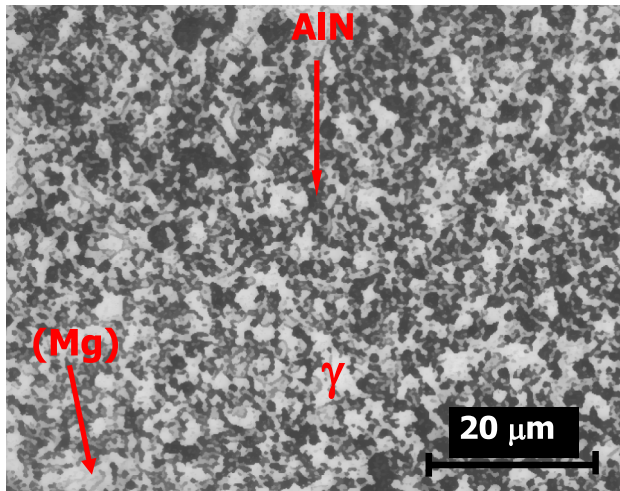


Fig. 11—OM of Mg-30 wt pct Al/AlN product for a flow rate of 0.1 LPM.

varying flow rate on the amount of AlN formed *in situ* in AlN-Mg alloy composites was investigated and results are discussed in the following section.

A. Effect of Flow Rate on AlN Yield

Effect of flow rate was studied by conducting experiments at two different flow rates of 0.04 and 0.1 LPM. The yield of AlN was calculated using XRD and EDS data. Figure 10 shows the effect of flow rate at temperature (1173 K), injecting time (70 minutes), and alloy composition (Mg-30 wt pct Al). As the flow rate increases, the amount of NH_3 passing through the alloy increases. As expected, the yield of AlN increased with increase in flow rate.

Figure 11 is an optical micrograph for injecting time of 70 minutes at a flow rate of 0.1 LPM of NH_3 . In this case the average AlN formed in the alloy was 27.43 wt pct. This AlN percentage is equal to 21.78 g of AlN formed in the starting alloy weight of 80 g (70 wt pct Mg-30 wt pct Al). The AlN particle size is not significantly varied with increasing flow rate. Due to lower yield of AlN for a flow rate of 0.04 LPM, Figure 9

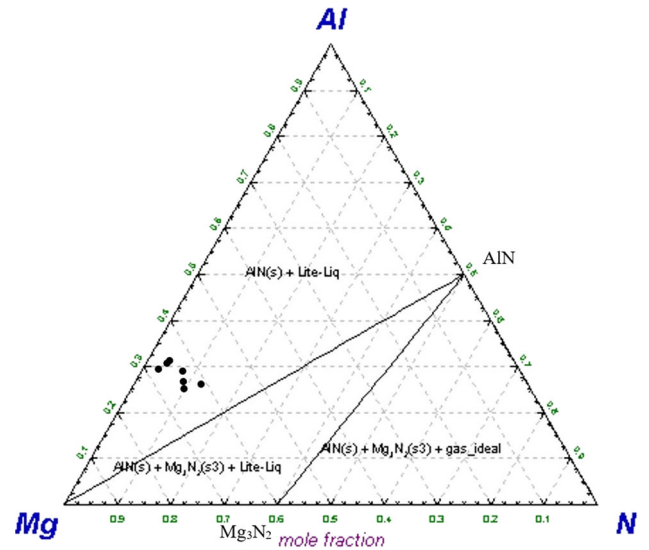


Fig. 12—Comparison of experimental results with Mg–Al–N ternary phase diagram at 1173 K.

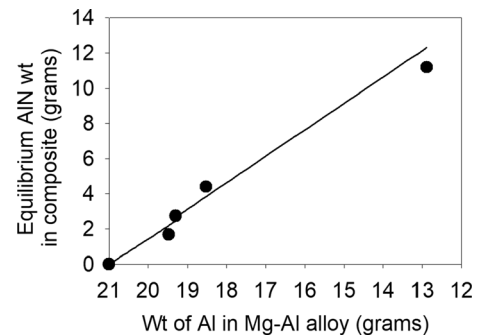


Fig. 13—Comparison of experimental with calculated equilibrium AlN data of Mg–Al–AlN at 1173 K for 0.04 LPM (solid line) thermodynamic calculated data and (black circle) experimental data.

shows lower dispersion density of AlN particles as compared to that at 0.1 LPM shown in Figure 11. Thus, it can be seen that flow rate is an important parameter in the synthesis of AlN-reinforced Mg-MMCs.

B. Comparison of Experimental Phases with Ternary Phase Diagram

The equilibrium composition of the final composites obtained from experiments was compared with the ternary phase diagram obtained using FactSage.^[39] The EDS data obtained based on an average measurement of 8 points for various process parameters at 1173K results are shown in Figure 12. All data points fall in the region in ternary diagram, where AlN and Mg–Al alloy are stable. This agrees with the thermodynamic modeling that Mg_3N_2 is not stable in the composite product, and as shown experimentally, the AlN is the only stable phase formed in the Mg–Al alloy composites with the injection of ammonia.

The equilibrium species distribution calculations for the Mg–Al alloy with ammonia gas were predicted using Gibbs energy minimization method.^[36,37] The effect of gas-injection time on species distribution at 1173 K at a flow rate of 0.04 LPM was studied experimentally. From the EDS analysis of the products produced, on absolute weight basis, the yield of AlN present in the alloy was calculated. Figure 13 shows the comparison of experimental and calculated equilibrium AlN data of Mg–Al–AlN system. As discussed above (Figure 10), the increase in injection flow rate of ammonia increases the amount of ammonia in the system. This increase in amount of ammonia increases the amount of N, which is available for the Al to react in the melt and results in the decrease of Al in the alloy and increases the formation of the amount of AlN in the Mg–Al alloy. Figure 13 shows a good agreement in modeled and experimental results which indicate that the formation AlN in Mg–Al alloy is achieved near equilibrium process.

V. CONCLUSIONS

AlN-reinforced Mg-MMCs can be synthesized using *in situ* gas-injecting method. Thermodynamic analyses showed that ammonia can be used as the gas precursor. Magnesium was found to decrease the oxygen content present in the system and thereby helping in achieving the expected low oxygen content for nitridation reactions. Using ammonia led to the formation of AlN in the Mg-30 wt pct Al melt at 1173 K. Average AlN content of 15.42 wt pct and 27.43 wt pct was formed in the product at a flow rate of 0.04 LPM and 1 LPM, respectively. AlN particles formed *in situ* are surrounded by the γ -phase. The yield of AlN was found to increase with an increase in the flow rate of ammonia. The equilibrium composition of the final composites obtained from experiments was compared with the constructed Mg–Al–N ternary phase diagram at 1173 K. All experimental data fall in the region in AlN and Mg–Al alloy ternary phase diagram, which is in confirmation with the thermodynamic prediction. The obtained equilibrium amount of AlN in composites as a function of Al content in alloy showed good agreement with the thermodynamic modeled and experimental results.

ACKNOWLEDGMENTS

The author is pleased to acknowledge the financial support for this research by the National Science Foundation and ACIPCO. The author is also pleased to thank Sumit Tyagi for conducting experimental work and the Department of Metallurgical and Materials Engineering (MTE) and The University of Alabama for providing experimental and analytical facilities.

CONFLICT OF INTEREST

On behalf of the author, the corresponding author states that there is no conflict of interest.

REFERENCES

1. L.M. Calado, M.J. Carmezim, and M.F. Montemor: *Front. Mater.*, 2022, vol. 8, p. 804906.
2. S. Dutta, S. Gupta, M. Roy, and A.C.S. Biomater: *Sci. Eng.*, 2020, vol. 6(9), pp. 4748–73.
3. R. Casati and M. Vedani: *Metals*, 2014, vol. 4, pp. 65–83.
4. M.A. Sazonov, T.A. Chernishova, and L.L. Rokhlin: *Konstr. I Funkc. Mater.*, 2010, vol. 2, pp. 3–22.
5. P.K. Rohatgi and B. Schultz: *Mater. Matter.*, 2007, vol. 4, pp. 16–21.
6. A.A. Luo: *J. Magnes. Alloys*, 2013, vol. 1, pp. 2–22.
7. H.Z. Ye and X.Y. Liu: *J. Mater. Sci.*, 2004, vol. 39, pp. 6153–71.
8. S.M. Arya and W.D. Griffiths: *Metall. Mater. Trans. B*, 2023, vol. 54B(4), pp. 1965–84.
9. G. Anbuechziyan, N.M. Mubarak, R.R. Karri, and M. Khalid: *Sci. Rep.*, 2022, vol. 12, p. 20053.
10. A.A. Luo: *Int. Mater. Rev.*, 2004, vol. 49, pp. 13–30.
11. K. Luo, L. Zhang, G. Wu, W. Liu, and W. Ding: *J. Magnes. Alloys*, 2019, vol. 7, pp. 345–54.
12. C.S. Kim, I. Sohn, M. Nezafati, J.B. Ferguson, B.F. Schultz, Z. Bajestani-Gohari, P.K. Rohatgi, and K. Cho: *J. Mater. Sci.*, 2013, vol. 48, p. 4191.
13. A.P. Khrustalyov, S.A. Vorozhtsov, I.A. Zhukov, V.V. Prokakhov, V.K. Dammer, and A.B. Vorozhtsov: *Russ. Phys. J.*, 2017, vol. 59, pp. 2183–85.
14. J.B. Ferguson, F. Sheykh-Jaberi, C.S. Kim, P.K. Rohatgi, and K. Cho: *Mater. Sci. Eng. A*, 2012, vol. 558, pp. 193–204.
15. M. Gupta and W.L.E. Wong: *Mater. Charact.*, 2015, vol. 105, pp. 30–46.
16. A. Luo: *Scr. Metall. Mater.*, 1994, vol. 31, pp. 1253–58.
17. N. Nagendra, B.S. Rao, and V. Jayaram: *Mater. Sci. Eng. A*, 1999, vol. 269, pp. 26–37.
18. H. Lianxi and W. Erde: *Mater. Sci. Eng. A*, 2000, vol. A278, pp. 267–71.
19. A. Luo: *Metall. Mater. Trans. A*, 1995, vol. 26A, pp. 2445–54.
20. Y. Cai, D. Taplin, M.J. Tan, and W. Zhou: *Scr. Mater.*, 1999, vol. 41(9), pp. 967–71.
21. R.A. Saravanan and M.K. Surappa: *Mater. Sci. Eng. A*, 2000, vol. A276, pp. 108–16.
22. A. Martin and J. Llorca: *Mater. Sci. Eng. A*, 1995, vol. A201, pp. 77–87.
23. D.M. Lee, B.K. Suh, B.G. Kim, and J.S. Lee: *Mater. Sci. Tech.*, 1997, vol. 13(7), pp. 590–96.
24. T. Ebert, F. Moll, and K.U. Kainer: *Powder Metall.*, 1997, vol. 40(2), pp. 126–30.
25. D. Magers and J. Willekens: *Processing Magnesium Alloys and Their Applications*, B.L. Mordike and K.V. Kainer: *Werkstoff-Informationsgesellschaft mbH, Frankfurt*, 1998, pp. 105.
26. R.G. Reddy: *Comput. Manufact.*, 1998, vol. 14(3), pp. 5–7.
27. G. Chu and M.K. Premkumar: *Metall. Mater. Trans. A*, 1993, vol. 24A(12), pp. 2803–05.
28. B. Wu and R.G. Reddy: *Metall. Mater. Trans. B*, 2002, vol. 33B, pp. 543–50.
29. Q. Zheng, B. Wu, and R.G. Reddy: *Adv. Eng. Mater.*, 2003, vol. 5, pp. 167–72.
30. Q. Zheng and R.G. Reddy: *J. Mater. Sci.*, 2004, vol. 39(1), pp. 141–49.
31. Q. Zheng and R.G. Reddy: *High Temp Mater. Proc.*, 2003, vol. 22(2), pp. 63–71.
32. Q. Zheng and R.G. Reddy: *Metall. Mater. Trans. B*, 2003, vol. 34B(6), pp. 793–804.
33. Q. Zheng and R.G. Reddy: *Aluminum 2003*, S. K. Das, TMS, Warrendale, PA, USA, 2003, pp. 87–96.
34. Q. Zheng, B. Wu, and R.G. Reddy: *State of Art in Cast Metal Matrix Composites in the Next Millennium: TMS Fall Meeting*, P.

- K. Rohatgi, TMS, Warrendale, PA, USA, 2000, vol. 2000, pp. 1–12.*
35. S. Tyagi, Q. Zheng, and R.G. Reddy: *Aluminum: S.K. Das, TMS 2004 Annual Meeting*, Charlotte, 2004, vol. 2004, pp. 63–72.
 36. N.A. Gokcen and R.G. Reddy: *Thermodynamics*, 2nd ed. Springer, New York, 1996.
 37. HSC Chemistry: thermodynamic software, copyright © Outokumpu Research Oy, Pori, Finland, A.Roine. 2022.
 38. X. Zheng, Q. Wang, M. Zhou, and C. Li: *Sci. China*, 2002, vol. 45(3), pp. 249–54.
 39. FactSage: Thermodynamic Software, copyright Thermfact 2002.
 40. C. Suryanarayana and M. G. Norton, *X-Ray Diffraction—A Practical Approach*, 98 Plenum Press, New York, 1998, pp. 227–34.

Publisher’s Note Springer Nature remains neutral with regard to jurisdictional claims in published maps and institutional affiliations.

Springer Nature or its licensor (e.g. a society or other partner) holds exclusive rights to this article under a publishing agreement with the author(s) or other rightsholder(s); author self-archiving of the accepted manuscript version of this article is solely governed by the terms of such publishing agreement and applicable law.